Icarus 226 (2013) 583–590

Contents lists available at SciVerse ScienceDirect

Icarus

journal homepage: www.elsevier.com/locate/icarus

# On the charge of nanograins in cold environments and Enceladus dust

N. Meyer-Vernet

*LESIA, Observatoire de Paris, CNRS, Université Pierre et Marie Curie, Université Denis Diderot, Meudon, France*

ARTICLE INFO

*Article history:*
Received 29 March 2013
Revised 10 June 2013
Accepted 10 June 2013
Available online 25 June 2013

*Keywords:*
Ices
Enceladus
Saturn, Satellites
Interplanetary dust

ABSTRACT

In very-low energy plasmas, the size of nanograins is comparable to the distance (the so-called Landau length) at which the interaction energy of two electrons equals their thermal energy. In that case, the grain's polarization induced by approaching charged particles increases their fluxes and reduces the charging time scales. Furthermore, for grains of radius smaller than the Landau length, the electric charge no longer decreases linearly with size, but has a most probable equilibrium value close to one electron charge. We give analytical results that can be used for nanograins in cold dense planetary environments of the outer Solar System. Application to the nanodust observed in the plume of Saturn's moon Enceladus shows that most grains of radius about 1 nm should carry one electron, whereas an appreciable fraction of them are positively charged by ion impacts. The corresponding electrostatic stresses should destroy smaller grains, which anyway may not exist as crystals since their number of molecules is close to the minimum required for crystallization.



## 1. Introduction

Dust particles of nanometric size have been detected in situ in various parts of the Solar System, e.g. near comets (Utterback and Kissel, 1990), in the Earth low ionosphere (e.g. Friedrich and Rapp, 2009 and references therein), in the solar wind near 1 AU (Meyer-Vernet et al., 2009), in streams ejected by Jupiter (Zook, 1996) and Saturn (Kempf et al., 2005), in the atmosphere of Saturn's moon Titan (Coates et al., 2007), and in the plume ejected by the icy moon Enceladus (Jones et al., 2009). Nanograins, which make the transition between molecules and bulk materials, can be produced by condensation of gases and aggregation of molecules (Kimura, 2012), and/or by fragmentation of larger dust (e.g. Mann and Czechowski, 2012). The large surface-to-volume ratio of nanoparticles makes the proportion of surface atoms significant, so that their characteristic properties often differ from those of bulk materials and they are major agents for interactions with particles and fields.

Nanograins play an important role in magnetized environments because their interaction with electromagnetic fields varies in proportion of their electric charge, which varies more slowly with size than do the friction forces (proportional to surface) and the gravitational forces (proportional to volume). Hence nanograins are generally driven by electromagnetic forces as are plasma particles, so that their electric charge governs their dynamics (e.g. Burns et al., 2001; Horanyi, 1996; Mann and Czechowski, 2012; Mann et al., 2013). The electric charge can also determine the grain's minimum size via the electrostatic stresses producing fracture, and it also affects the grains' growth and coalescence. At larger scales, it determines the Larmor frequency and thus the time scale of grains' pick-up.

At nanometric sizes, several effects make the charging processes different from the classical charging of larger objects. First, it is well known that the particle sticking coefficients and photoelectric and secondary emission yields can change (Watson, 1972; Chow et al., 1993; Weingartner and Draine, 2001; Abbas et al., 2010; Mann et al., 2011), essentially because the electron free path in matter is of the order of (or larger than) 1 nm below ~10 eV (Fitting et al., 2001).

Two further effects appear when the grain radius becomes comparable to

$$r_L = e^2/(4\pi\epsilon_0 k_B T) \quad (1)$$

in a plasma of temperature $T$. Since $r_{L(\mathrm{nm})} \simeq 1.44/T_{\mathrm{eV}}$, this concerns nanograins in plasmas of temperature ≃1 eV. This scale, often called the Landau radius, is the distance below which the mutual electrostatic energy of two approaching charged particles exceeds the kinetic energy of their relative motion, so that they significantly perturb each other's trajectories. This fundamental scale, which determines the plasma particle cross-sections for Coulomb collisions producing large perturbations, is also of major importance for dust grains. Indeed, the particles approaching a grain of radius $\sim r_L$ or smaller induce polarization charges whose Coulomb attraction increases the collected fluxes, thereby decreasing the charging time scales. Furthermore, since at this scale the charging becomes discretized, the equilibrium charge on a grain no longer varies in

*E-mail address:* nicole.meyer@obspm.fr
*URL:* http://www.lesia.obspm.fr/perso/nicole-meyer/

0019-1035/$ - see front matter © 2013 Elsevier Inc. All rights reserved.
http://dx.doi.org/10.1016/j.icarus.2013.06.014

proportion of its size, but becomes comparable to one electron charge in a wide range of sizes, because the probability that an uncharged grain collects an electron exceeds the probability that a neutral or negatively charged grain collects an ion.

The latter phenomena have been studied in the contexts of the Earth's ionosphere (e.g. Jensen and Thomas, 1991; Rapp and Lübken, 2001 and references therein) and of the interstellar medium (e.g. Draine and Sutin, 1987; Weingartner and Draine, 2001). In this paper, we consider these effects for cold dense planetary environments in the outer Solar System, which are subjected to different constraints. We derive analytical results that can be used in these contexts, and apply them to the nanograins detected in Enceladus plume (Jones et al., 2009; Hill et al., 2012), where the electrons are cold enough (Shafiq et al., 2011) to put the Landau radius in the nano range, the plasma is dense enough (Morooka et al., 2011) for the photoelectron emission to be negligible, and the (larger) dust concentration is high enough to deplete the electrons by a large amount.

These calculations will enable us to estimate the grains' size limit set by electrostatic disruption and to compare it with other physical processes.

Units are SI, unless otherwise indicated explicitly.

## 2. Basic impact charging

Before considering nanograins, let us briefly summarize the classical electric charging by collection and emission of particles for a dust grain of radius $a \gg r_L$ in a plasma whose electron and ion densities may be different because of the possible presence of dust.

### 2.1. Impacts of charged particles

The charging of a grain changes its electric potential, which changes the particle fluxes until an equilibrium is reached when the different charge fluxes balance each other. The electron flux tends to exceed that of ions because of the faster electron speeds (except in the case of strong electron depletion discussed in Section 2.3); hence, when the charging is mainly due to electron and ion impacts, the body charges negatively until it repels sufficiently the electrons for their flux to balance that of positive ions. For this to be so, the electron potential energy at the body's surface $e\Phi$ must exceed sufficiently (but not too much) the particle thermal energy $\sim k_B T$. Thus the equilibrium grains' potential with respect to the ambient plasma is $\Phi \simeq -\eta k_B T/e$, with $\eta$ of order of magnitude unity. For a sphere of radius $a$ much smaller than both the Debye length $L_D$ and the grains' separation, the electric charge is $Q = 4\pi\epsilon_0 a\Phi$. Substituting the above value of $\Phi$ yields the number of charge units $Q/e$ at equilibrium

$$Z = -\eta a/r_L \tag{2}$$

with $\eta \sim 1$ in order of magnitude. The mean number of a grain's charges thus exceeds unity when $a/r_L \gg 1$.

The parameter $\eta$ is easily calculated since in that case the particles are subjected to the Coulomb potential of the grain without intervening barriers of potential (the so-called orbit-limited condition (Laframboise and Parker, 1973; Whipple, 1981)). When the plasma particles are singly charged and have isotropic Maxwellian velocity distributions, the classical fluxes of each particle species can then be expressed straightforwardly as

$$N = N_0 e^{-|\eta|} = N_0 e^{-|Z|r_L/a} \quad \text{repelled particles} \tag{3}$$

$$N = N_0(1 + |\eta|) = N_0(1 + |Z|r_L/a) \quad \text{attracted particles} \tag{4}$$

per unit grain's surface, where $r_L$ is the Landau radius corresponding to the temperature of the species considered and $N_0$ is the flux of that species on an uncharged grain

$$N_0 = sn\langle v\rangle/4 = sn(k_B T/2\pi m)^{1/2} \tag{5}$$

Here $s$, $n$, $T$, $m$, and $\langle v\rangle$ are the sticking probability, number density, temperature, mass, and mean speed of the species concerned in the unperturbed plasma. For ions of mass $m_i$ and same temperature $T$ as electrons of mass $m_e$, we have

$$N_{0e}/N_{0i} = \mu(n_e/n_i) \quad \text{with } \mu = (s_e/s_i)(m_i/m_e)^{1/2} \tag{6}$$

At equilibrium, the electron and ion fluxes balance, and $\eta$ is the solution of the equation

$$\eta = \ln[\mu(n_e/n_i)/(1+\eta)] \tag{7}$$

This confirms that $\eta$ is of order of magnitude unity, except if $\mu(n_e/n_i) \simeq 1$ – a case that we will discuss later. Note that we have not assumed $n_e = n_i$, in order for the results to be applicable in dusty environments. Therefore, although $\mu \gg 1$ because of the large ion-to-electron mass ratio, we have not necessarily $\mu(n_e/n_i \gg 1$, but only the weaker inequality $\mu(n_e/n_i) > 1$ (as will be shown in Section 2.3).

For nanograins in a low-energy plasma, the sticking probability of ions $s_i \simeq 1$, but the sticking probability of electrons may be smaller because the free path of electrons in solids (which decreases as energy decreases at energies exceeding a few 100 eV) reaches a minimum generally smaller than 1 nm in the vicinity of tens eV, and increases as energy decreases again to values comparable to or greater than 1 nm around 1 eV, taking into account elastic and inelastic scattering (Fitting et al., 2001). A conservative assumption is $s_e \simeq 0.3$–1 (Jurac et al., 1995; Vostrikov and Dubov, 2006; Megner and Gumbel, 2009) for nanograins, keeping in mind that $s_e$ may be much smaller as the number of atoms decreases (Michaud and Sanche, 1987), essentially because the limited number of degrees of freedom precludes the conservation of energy and momentum in the collision.

For water-group incident ions $\mu \simeq 180 \times s_e$, so that Eq. (7) yields $\eta \simeq 0.31$, 1.85, or 3.65 for respectively $s_e n_e/n_i = 0.01$, 0.1, or 1.

### 2.2. Other charging processes

The above estimates assume that photoemission (including photodetachment) and secondary emission are negligible. The photoelectron emission on uncharged grains at heliospheric distance $r_{\rm AU}$ (in astronomical units) can be approximated by (Grard, 1973)

$$N_{ph0} \simeq 0.5 \times 10^{14}\chi/r_{\rm AU}^2 \quad \chi \sim 0.1{-}1 \tag{8}$$

per unit of the total grain's surface area $4\pi a^2$ – to facilitate comparison with other fluxes (we have taken into account that the projected sunlit area is one-quarter of the grain's surface area). The smaller value of $\chi$ corresponds for example to materials such as graphite or ice, the larger to silicates.

For nanograins $\chi$ may be different for two main reasons which act in opposite senses. First, since the photon attenuation length generally exceeds the photoelectron escape length by a large amount, a small grain size limits the distance from the excitation region to the surface, which tends to increase the yield compared to that of bulk materials (Watson, 1972; Weingartner and Draine, 2001). Second, the photon absorption cross-section (normalized to the cross-sectional area) at the relevant wave lengths $\lambda \sim 0.1$ μm varies roughly as $2\pi a/\lambda \simeq 6 \times 10^{-2} a_{\rm nm}$ when this size parameter is much smaller than unity; this is expected to decrease $\chi$ significantly. Because of the large uncertainties in these properties, we will use the conservative assumption $\chi \leqslant 0.1$ for silicate and water ice nanograins. From (8), we deduce the ratio between photoelectron emission and ion (of mass $Am_p$) collection for uncharged grains at 10 AU heliocentric distance (≃Saturn's orbit),

$$N_{ph0}/N_{0i} \leqslant 13A^{1/2}/(n_{i(\mathrm{cm}^3)}T_{i(\mathrm{eV})}) \quad (9)$$

Photoelectron emission is thus expected to be of minor importance for water-group incident ions of density $n_i \geqslant 50\ \mathrm{cm}^{-3}$ and temperature $\sim$1 eV. Likewise, "true" secondary electron emission is expected to be negligible, even for very small grains, for electron temperatures $\sim$1 eV (Chow et al., 1993).

The above calculations assume for simplicity that the particle velocity distributions are Maxwellian. Solar System plasmas are generally non-maxwellian, containing suprathermal particles with Kappa-like distributions (Garrett and Hoffman, 2000; Meyer-Vernet, 2001; Pierrard and Lazar, 2010). This changes the fluxes (Mendis and Rosenberg, 1994) and might have large consequences if the secondary electron emission were not negligible (Meyer-Vernet, 1982; Chow et al., 1993). The grain relative velocity has also been neglected, which is acceptable if it is smaller than the ion thermal speed.

### 2.3. Dusty environments

Finally, let us discuss briefly how the plasma electron depletion $n_e/n_i$ is related to the charged dust. Strictly speaking, the above calculations hold when the dust grains are "isolated", thus when the grains' number density $n_d$ is small enough that their separation exceeds twice the Debye length, i.e. $2n_d^{1/3}L_D < (3/4\pi)^{1/3}$. With the grains' charge (2) and the Debye length

$$L_D = [4\pi r_L(n_e + n_i)]^{-1/2} \quad (10)$$

the ratio of the charge carried by the grains to that available in the medium is $|Z|n_d/(n_e + n_i) \simeq \eta P$ with

$$P \equiv 4\pi n_d a L_D^2 \quad (11)$$

Since $P < \left(2n_d^{1/3}L_D\right)^2$ because the grains' separation necessarily exceeds their diameter, we have $P < 1$ if the grains' separation exceeds $L_D$, so that in that case the grains' charge is not expected to perturb significantly the plasma.

In the opposite case $P > 1$, the grains' Debye spheres overlap and the electrons are depleted since many of them rest on the grain's surface, which in turn reduces the grain's charge (Havnes et al., 1984; Whipple et al., 1985). However, if the grain size is much smaller than the grains' separation, the increase of the grain-to-plasma capacitance due to the neighboring grains can be neglected and Eqs. (3) and (4) still hold (Whipple et al., 1985), with $\eta \equiv -e\Phi/k_BT = -Zr_L/a$ where $\Phi$ is the grain-to-plasma potential. Therefore (7) holds in that case and using the quasi-neutrality condition $n_i - n_e = -n_dZ$ and rewriting (10) as $n_i + n_e = n_d a/P\, r_L$, one deduces straightforwardly

$$\frac{n_e}{n_i} = \frac{(1+\eta)e^{\eta}}{\mu} = \frac{1 - P\eta}{1 + P\eta} \quad (12)$$

From (12), one can deduce two of the three parameters $n_e/n_i$, $\eta$, and $P$, from one of them. Fig. 1 shows $n_e/n_i$ versus $P$, which enables one to deduce the grains' properties from the electron depletion or vice versa. For completeness we have also plotted $\eta$ versus $P$, first published by Whipple et al. (1985) and reproduced in several papers. Note that the pioneering results by Havnes et al. (1984, 1990) and references therein use a different definition of $P$, based on the plasma properties outside the dusty region – which is relevant for studying the local properties of a dust cloud; both definitions agree in the limit of small potentials (when the Boltzmann factors can be linearized).

In the limit $P \to \infty$, (12) yields

$$n_e/n_i \simeq 1/\mu \quad \eta \simeq 1/P \to 0 \quad (13)$$

which corresponds to the limit $\mu n_e/n_i \to 1$ of Eq. (7) and shows that the electrons cannot be more depleted with respect to ions than the limiting value $n_e/n_i \simeq 1/\mu$ (Mendis and Rosenberg, 1994).

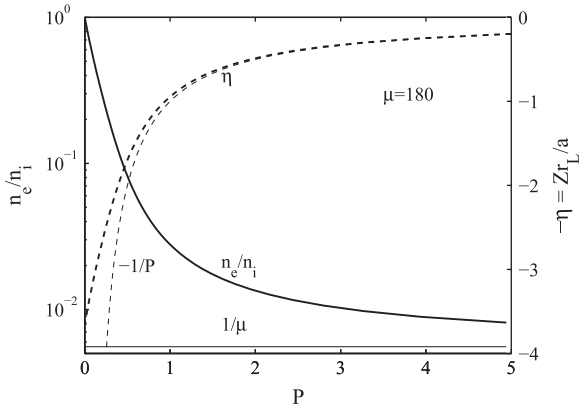


**Fig. 1.** Electron-to-ion number density $n_e/n_i$ (left axis, solid line) and normalized grain's charge $-\eta = Zr_L/a$ (right axis, dashed) versus the parameter $P = 4\pi n_d\langle a\rangle L_D^2$, from (12) with $\mu = 180$ (water-group ions and electron sticking probability $s_e \simeq 1$) for dust grains of radius $a > r_L$. The limits $n_e/n_i \sim 1/\mu$ and $\eta \sim 1/P$ for $P \to \infty$ are plotted for comparison (thin lines).

Of course, when the grains have a continuous size distribution $dn_d/da$ (for $a_{\min} < a < a_{\max}$), $P$ must be calculated by replacing in (11) $a$ by its mean value $\langle a\rangle = \int_{a_{\min}}^{a_{\max}} da a(dn_d/da)/n_d$ (Havnes et al., 1990). In general the minimum $a_{\min}$ is unknown, but dust analyzers can measure the number density $n_d(a_0)$ of grains larger than some radius $a_0 > a_{\min}$. In that case, one can derive $a_{\min}$ from the measured value of $n_e/n_i$ without having to make a hypothesis on the grains' potential. For example, with $dn_d/da \propto a^{-p}$ (with $p > 2$) so that the number density of grains larger than $a$ is $n_d(a) \propto a^{1-p}$, we substitute $\langle a\rangle$ for $a$ in (11) and get

$$a_{\min} = \left(\frac{4\pi L_D^2}{P}\frac{p-1}{p-2}n_d(a_0)a_0^{p-1}\right)^{1/(p-2)} \quad (14)$$

which together with (12) yields $a_{\min}$ as a function of $n_e/n_i$. This will be used in Section 5.

## 3. Grains' polarization

The results of Section 2 hold for grains of size much larger than the Landau radius; how much larger will be determined later (Eq. (39) and Fig. 3). For smaller grains, the polarization charges induced on a grain by approaching charged particles produce an electric potential which perturbs significantly their trajectories, as first shown in the context of ion capture by aerosols in the Earth's ionosphere (Natanson, 1960); hence the particle fluxes are modified.

Consider an ion or an electron (charge $\pm e$) approaching at distance $r = ax$ from the centre of a spherical grain of radius $a$ and electric charge $Ze$. The approaching particle is subjected to an electrostatic field that can be derived from the potential

$$\Phi(r) = \frac{e}{4\pi\epsilon_0 a}\left[\frac{Z}{x} \mp \frac{1}{2x^2(x^2-1)}\right] \quad x = r/a \quad (15)$$

obtained by adding to the Coulomb potential of the grain's charge that of the induced image (Jackson, 1999).

### 3.1. Uncharged grains

Consider first an uncharged grain ($Z = 0$). Plasma particles of charge $\pm e$ are subjected to the image term of the potential (15), so that they are all attracted and their trajectories are bent towards the grain. Consider particles arriving isotropically from large distances at speed $v$. The impact parameter $p$ of the trajectory which

barely grazes a sphere of radius $r$ is given by conservation of energy and momentum (in spherical coordinates) as

$$p^2/a^2 = x^2 + x_v/[2(x^2-1)] \quad x = r/a \tag{16}$$

$$\text{where} \quad x_v = [e^2/(4\pi\epsilon_0 m v^2/2)]/a \tag{17}$$

For $r/a \to \infty$, (16) yields $p \to r$, as expected since the image potential becomes negligible at large distances and produces straight lines trajectories; at small distances, the trajectories are bent by the image force and for $r/a \to 1$ we have $p/a \to \infty$ because of the increasing bending of the trajectories as the image term in (15) increases. Between these two extremes, $p$ has a minimum $p_0$ obtained from (16) by noting that $dp/dx = 0$ for $(x^2-1)^2 = x_v/2$, whence $p_0^2/a^2 = 1 + \sqrt{2x_v}$. The particle random flux $snv/4$ is therefore increased by the factor $p_0^2/a^2$, which yields the flux $N_v = sn[v + e(\pi\epsilon_0 m\ a)^{-1/2}]/4$. Averaging over speeds and using $\langle v\rangle = (8k_BT/\pi m)^{1/2}$ yields the flux

$$N = N_0 F_0 \quad \text{for} \quad Z = 0 \tag{18}$$

$$F_0 = 1 + (\pi r_L/2a)^{1/2} \tag{19}$$

This exceeds the flux $N_0$ given by (5) by the factor $F_0$, which may be very large when $a \ll r_L$.

### 3.2. Repelling grains

Now, consider particles which are repelled at distances $r \gg a$ (electrons if $Z < 0$ or positive ions if $Z > 0$). In that case, the two terms in the potential (15) are of opposite signs so that the potential has a maximum at the distance $r_0$ given by

$$2x_0^2 - 1 = |Z|x_0(x_0^2-1)^2 \quad x_0 = r_0/a \tag{20}$$

For $Z = 1$ and 2, (20) yields $x_0 \simeq 1.62$ and 1.42 respectively, whereas in the limit $|Z| \to \infty$ we have $x_0 \simeq 1 + 0.5|Z|^{-1/2}$. At the maximum of the barrier of potential, the potential energy of the charge $\pm e$ is

$$\pm e\Phi(r_0) = \frac{|Z|e^2}{4\pi\epsilon_0 a}\left[\frac{1}{x_0} - \frac{|Z|^{-1}}{2x_0^2(x_0^2-1)}\right] \tag{21}$$

For $Z \to +\infty$, the expansion of the bracket in (21) to first order in $|Z|^{-1/2}$ yields $[1 - |Z|^{-1/2}]$, whereas for $Z = 1$ and 2 the bracket $\simeq 1/[1 + |Z|^{-1/2}]$. Hence a reasonable approximation of (21) is

$$\pm e\Phi(r_0) \simeq \frac{1}{4\pi\epsilon_0 a}\frac{|Z|e^2}{1+|Z|^{-1/2}} \tag{22}$$

As soon as the approaching particles come closer than $r_0$, they are attracted. Hence the effective collection radius is increased by a factor $y_0^2$, with $y_0 \simeq x_0$ for $x_0 \gg 1$ since in that case the particles are weakly affected by the grain's charge farther than $r_0$. In the general case we have $y_0 < x_0$ because of the repelling electric force farther than $r_0$. Since only particles of kinetic energy exceeding $|e\Phi(r_0)|$ can reach this distance, the flux of repelled particles with a Maxwellian distribution of temperature $T$ is given by

$$N = N_0 y_0^2 e^{-|e\Phi(r_0)|/k_BT} \simeq N_0 F_r(Z) \quad \text{repelled particles} \tag{23}$$

$$F_r(Z) \simeq [1 + (3|Z| + 4a/r_L)^{-1/2}]^2 e^{-\left(\frac{|Z|r_L/a}{1+|Z|^{-1/2}}\right)} \tag{24}$$

where we have used an approximation of $y_0$ derived by Draine and Sutin (1987). Comparing with (3), one sees that the polarization increases significantly the flux of repelled particles, by a factor $\simeq 2.6 \times e^{r_L/2a}$ for $|Z| = 1$ and $a/r_L \ll 1$, which can be quite large for very small grains.

### 3.3. Attracting grains

Finally, consider particles which are attracted at distances $r \gg a$ (positive ions if $Z < 0$ or electrons if $Z > 0$). In that case the focusing has two causes: first, the field of the grain's charge $Ze$ which would yield the flux (4) in the absence of polarization and acts far from the grain; second, the image contribution which would yield the flux (18) when $Z = 0$ and acts close to the grain. By comparing (4) and (18), one sees that the attraction of the grain's charge generally dominates, so that the flux is given by (4) with a correcting factor. Using an approximation for this factor (Draine and Sutin, 1987), one obtains for a Maxwellian distribution at temperature $T$

$$N = N_0 F_a(Z) \quad \text{attracted particles} \tag{25}$$

$$F_a(Z) = (1 + |Z|r_L/a)[1 + (|Z| + a/2r_L)^{-1/2}] \tag{26}$$

We conclude that when the grain's size does not exceed the Landau radius by a large amount, the polarization increases the fluxes whatever the grain's charge, thereby decreasing the charging time scales. Furthermore, because the flux of repelled particles is increased by a larger factor than the other ones because of the exponential term, the negative equilibrium charge tends to increase. However, since in that case $|Z|$ is not large, a statistical treatment of the grain charge distribution is needed.

## 4. Charge probability distribution

### 4.1. Charge probabilities

Let $f(Z)$ be the probability that a grain carries the charge $Ze$. The population of grains of charge $Ze$ is depleted by collecting electrons and ions and replenished when grains of charge $(Z+1)e$ collect electrons and when grains of charge $(Z-1)e$ collect ions (as discussed in Section 2, we neglect secondary or photoelectron emission). Under stationary conditions, this yields the simple recurrence relation (Draine and Sutin, 1987)

$$f(Z)N_i(Z) = f(Z+1)N_e(Z+1) \tag{27}$$

equivalent to a more complicated relation used by (Rapp and Lübken, 2001). Applying (27) iteratively with $N_e(Z)$ and $N_i(Z)$ given by (18) for $Z = 0$ and respectively by (23) and (25) for $Z < 0$ and the reverse for $Z > 0$, we obtain

$$f(Z)/f(0) = (\mu n_e/n_i)^{|Z|} F_0 \prod_{Z'=Z}^{-1}\left[\frac{F_r(Z'+1)}{F_a(Z')}\right] \quad Z < 0 \tag{28}$$

$$f(Z)/f(0) = (\mu n_e/n_i)^{-Z} F_0 \prod_{Z'=1}^{Z}\left[\frac{F_r(Z'-1)}{F_a(Z')}\right] \quad Z > 0 \tag{29}$$

where $F_0$, $F_r$, $F_a$ are defined respectively in (19), (24), (26), and we set $F_r(0) = 1$ in (28). This can be solved by using $\sum_{-\infty}^{+\infty} f(Z) = 1$.

### 4.2. Singly charged grains

Eqs. (28) and (29) yield in particular

$$\frac{f(-1)}{f(0)} \simeq (\mu n_e/n_i)\frac{1 + (\pi r_L/2a)^{1/2}}{(1 + r_L/a)[1 + (1 + a/2r_L)^{-1/2}]} \tag{30}$$

$$\frac{f(-1)}{f(+1)} \simeq (\mu n_e/n_i)^2 \tag{31}$$

Two important consequences emerge. First, since $\mu \gg 1$ because of the large ion-to-electron mass ratio, the positive grains are in minority but they may be detectable, the more so as the electrons are significantly depleted. Second, in the limit $a \ll r_L$, (30) yields $f(-1)/f(0) \simeq (\mu n_e/n_i)(\pi a/8r_L)^{1/2}$, an approximation which turns out to be accurate to within 5% in the whole range $a/r_L \leqslant 1$.

For small grains the probability is concentrated on the states $Z = 0$ and -1 since the number of negative charges is not only limited by the exponential factor in (23), but also by electron field

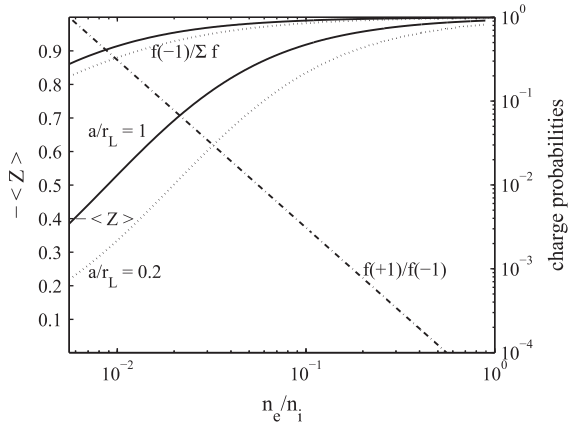


**Fig. 2.** Mean number of grain charge units $\langle Z\rangle$ (left axis), proportion of negatively charged grains $f(-1)/\sum f$ (right axis) and ratio of positively to negatively charged grains (dash-dotted, right axis) versus the electron-to-ion number density $n_e/n_i$ for two values of $a/r_L$ with $\mu = 180$ (water-group ions with $s_e \simeq 1$). These results concern grains of radius smaller than 1 nm for which the electron field emission limit (32) prevents multiple negative charging.

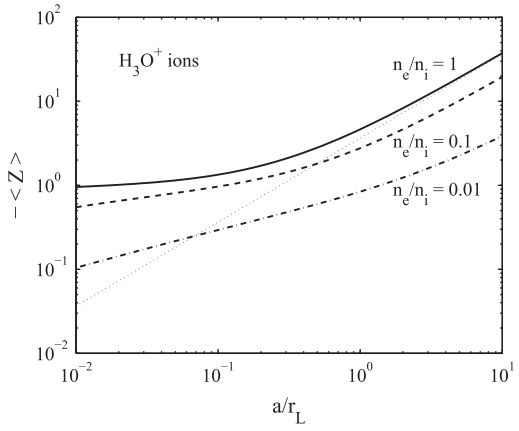


**Fig. 3.** Mean equilibrium number of electrons carried by a grain from (39) versus its normalized radius, for different values of the electron-to-ion number density and $\mu = 180$ (water-group ions with electron sticking coefficient $s_e \simeq 1$). The classical value $-\langle Z\rangle = 3.65a/r_L$ is plotted (light dotted) for comparison. These values do not take into account the electron field emission limit, which prevents multiple charging for grains of radius smaller than about 1 nm.

emission (e.g. Mendis and Axford, 1974; Draine and Sutin, 1987). Indeed, for nanograins we have $e^2/4\pi\epsilon_0 a \simeq 1.4$ eV, so that the surface Coulomb electric field deforms significantly the potential barrier at the surface, which enables electrons inside to tunnel efficiently. In practice, this process becomes efficient when $|E| > 10^9$ V/m (Gomer, 1961). An ejected electron near the surface of a grain of charge $Ze < 0$ will be subjected to the field amplitude $|E| \simeq (Z+1)e/4\pi\epsilon_0 a^2$. Hence the condition $|E| < 10^9$ V/m for electron field emission not to occur limits the grain charge state to

$$Z > -(1 + 0.7a_{nm}^2) \quad \text{Field emission limit} \tag{32}$$

We do not consider ion field emission which limits the positive charging, since it requires a much higher field.

For $a \leqslant 1$ nm, electron field emission thus limits the (integer) number of grain charges $Q/e$ to $Z \geqslant -1$, as noted by Hill et al. (2012). Hence, the probability is concentrated on the states $Z = 0$ and $-1$, and the mean grains' charge number at equilibrium is $\langle Z\rangle \simeq -f(-1) = -1/[1 + f(0)/f(-1)]$, i.e.

$$\langle Z\rangle \simeq \frac{-1}{1 + (8r_L/\pi a)^{1/2}/(\mu n_e/n_i)} \tag{33}$$

$$\simeq -\left[1 + \frac{10^{-2} n_i/s_e n_e}{(a_{\rm nm} T_{\rm eV})^{1/2}}\right]^{-1} \tag{34}$$

Therefore, the mean equilibrium charge of grains of radius $a \simeq 1$ nm in a plasma of temperature $\simeq$1 eV is roughly one electron if $s_e n_e/n_i \gg 10^{-2}$, and the ratio of positive to negative grains is according to (30)

$$f(+1)/f(-1) \simeq (5 \times 10^{-3} n_i/s_e n_e)^2 \tag{35}$$

These values are plotted in Fig. 2. They hold at equilibrium. The charging time scales can be estimated from the electron and ion flux on an uncharged grain, respectively, given from (18) and (19), which yield

$$\tau_{-1} \simeq \left[4\pi a^2 n_e s_e \left(\frac{k_B T_e}{2\pi m_e}\right)^{1/2} \left(1 + \left(\frac{\pi r_L}{2a}\right)^{1/2}\right)\right]^{-1} \tag{36}$$

$$\simeq \left[2 \times 10^{-6} s_e n_{\rm ecm^{-3}} a_{\rm nm}^2 \left(T_{\rm eV}^{1/2} + \frac{1.5}{a_{\rm nm}^{1/2}}\right)\right]^{-1} \text{s} \tag{37}$$

$$\tau_{+1} \simeq (\mu n_e/n_i) \times \tau_{-1} \tag{38}$$

### 4.3. Average charge of small or large grains

Using (33) (valid for small grains) and (2) with (7) (valid for large grains), we obtain the general approximation

$$\langle Z\rangle \simeq -\eta_0 a/r_L - \frac{1}{1 + 0.9 \times 10^{-2}(n_i/n_e)(r_L/a)^{1/2}} \tag{39}$$

for water-group incident ions, with $\eta_0$ solution of $e^{\eta_0}(1+\eta_0) \simeq 180 n_e/n_i$ and $s_e = 1$; if $s_e < 1$, $n_e/n_i$ must be multiplied by $s_e$ in these expressions. A similar approximation was studied by Draine and Sutin (1987) in the special case $n_e = n_i$. Eq. (39) is plotted in Fig. 3 for several values of $n_e/n_i$ and compared to the classical result valid for $a \gg r_L$ and $n_e \simeq n_i$ (dotted).

Two further consequences emerge. First, the quasi-neutrality condition $n_e - n_i = n_d Z$ no longer yields (12) for grains of radius $a \lesssim r_L$ since in that case $\langle Z\rangle$ is no longer given by the first term of (39); one can nevertheless apply (12) in the Enceladus plume for larger grains, since they carry most of the dust total charge (Dong and Hill, 2012). Second, the grains' charge-to-mass ratio, which governs their dynamics, varies faster with mass for smaller grains. Indeed, whereas the charge-to-mass ratio of large grains varies in proportion of $Z/a^3 \propto 1/a^2$ (from the dominant first term in (39)), the charge-to-mass ratio of smaller grains varies faster when the second term in (39) is dominant; if $n_e/n_i \simeq 10^{-2}$ this occurs as soon as $a \lesssim 10 r_L$, whereas if $n_e/n_i \simeq 1$, the charge-to-mass ratio goes as $1/a^3$ for $a < r_L$.

## 5. Enceladus nanograins

Consider nanograins in the Enceladus plume, almost at rest (Tokar et al., 2009) with respect to Enceladus as well as with respect to the plasma, of typical parameters: $n_i \sim 10^3 - 3 \times 10^4$ cm$^{-3}$, $n_e/n_i \sim 10^{-2} - 10^{-1}$, $T \sim 1$ eV (Morooka et al., 2011; Shafiq et al., 2011), main ion $H_3O^+$ (Cravens et al., 2009) and with a neutral gas density $n_0 \sim 5 \times 10^7$ cm$^{-3}$ (Waite et al., 2006). This yields the Landau radius $r_L \simeq 1.4$ nm and the Debye length $L_D \simeq 0.07 \leftrightarrow 0.23$ m for $n_i \sim 10^4 \leftrightarrow 10^3$ cm$^{-3}$ respectively.

### 5.1. Negatively charged nanograins

We deduce from (34) (see also Fig. 2) that more than 50% of the grains of radius $a \simeq 1$ nm should carry one electron at equilibrium

provided that $n_e/n_i > 10^{-2}/s_e$ ($s_e$ being the electron sticking probability), which confirms the value inferred for these grains (Hill et al., 2012).

The corresponding charging time scale is given by (37), which yields $\tau_{-1} \simeq 200 \leftrightarrow 2000$ s for $n_e s_e \sim 10^3 \leftrightarrow 10^2$ cm$^{-3}$ respectively. Note that neglecting the grains' polarization would yield charging time scales roughly twice larger than these values. With a speed $\simeq$0.5 km/s with respect to Enceladus – of the order of the gas bulk speed (Hansen et al., 2008; Dong et al., 2011), this yields the free path for negative charging $\simeq 0.4 \leftrightarrow 4R_E$ (Enceladus radius $R_E \simeq 250$ km). This confirms the order-of-magnitude estimate by Hill et al. (2012) indicating that these nanograins are charged by the ambient plasma.

### 5.2. Positively charged nanograins

Consider now the observed positively charged grains (Jones et al., 2009; Hill et al., 2012), whose origin is under debate. Hill et al. (2012) suggested three possible mechanisms: secondary electron emission, impacts of positive ions, and triboelectric charging (the latter first suggested by Jones et al. (2009)). The results of Section 4 enable us to estimate the grains' charging states resulting from the flux of ambient electrons and ions (taking into account the grains' polarization and charge discretization). According to (35), we have $f(+1)/f(-1) \sim (5 \times 10^{-3} n_i/s_e n_e)^2 \sim 2 \times 10^{-1} \leftrightarrow 2 \times 10^{-3}$ for $n_e/n_i \sim 10^{-2} \leftrightarrow 10^{-1}$ respectively (for $s_e \sim 1$). Since, according to (32), grains of radius $a \simeq 1$ nm or smaller do not carry more than one electron, $f(+1)/f(-1)$ yields the ratio of positively to negatively charged grains. However this is an equilibrium value, which holds when the time involved exceeds the larger charging time scale $\tau_{+1}$; otherwise, the ratio $f(+1)/f(-1)$ should be smaller since $\tau_{+1} > \tau_{-1}$. With $n_i \simeq 3 \times 10^4$ cm$^{-3}$, (38) yields $\tau_{+1} \simeq 1300$ s. With a speed $\simeq$0.5 km/s, this yields a free path for (positive) charging $\simeq 2R_E$. This value is of the order of the involved paths, which suggests that a significant proportion of these nanograins have their equilibrium charge. These estimates are a strong indication that the impacts of ambient plasma particles can explain both the negatively and positively charged grains, without having to rely on other charging processes.

### 5.3. Electron depletion

The charge of these nanograins cannot compensate for the strong observed electron depletion, and larger grains act to achieve plasma quasi-neutrality (Yaroshenko et al., 2009; Farrell et al., 2010). When those "large grains" represent the major contribution to the total dust charge, Fig. 1 (Eq. (12)) enables one to deduce directly their properties from the observed electron depletion or vice versa, via $P$. For example, let us assume $dn_d/da \propto a^{-p}$ for $a > a_{min}$ with $p = 4.5$ and a number density $n_d(a_0) \simeq 0.1$ cm$^{-3}$ for grains of radius $a_0 > 2$ μm, according to typical measurements (Spahn et al., 2006; Kempf et al., 2008). Eqs. (12) and (14) show that with an observed electron depletion $n_e/n_i \simeq 10^{-2}$, quasi-neutrality can be achieved with $a_{min} \simeq 0.1$ μm. Note that this estimate does not require the grain potential as an input since it is calculated in parallel, contrary to estimates using the measured spacecraft potential (e.g. Shafiq et al., 2011).

Finally, according to Eq. (13), the electrons cannot be more depleted than $n_e/n_i \simeq 1/\mu \simeq 5 \times 10^{-3}/s_e \geqslant 5 \times 10^{-3}$ (since $s_e \leqslant 1$), which agrees in order of magnitude with observation.

### 5.4. Minimum size of nanograins

Finally, consider grains of radius smaller than about 1 nm. According to (34), their charge should decrease below one charge unit when $a_{\rm nm} < (10^{-2} n_i/s_e n_e)^2/T_{\rm eV}$, whereas their charging time scale increases. This might possibly contribute to the decrease observed in the flux of charged grains below 1 nm (Hill et al., 2012; Jones et al., 2012).

Several other effects are expected to act at such small sizes. First, the high electric field $E_0 = Ze/4\pi\epsilon_0 a^2$ at the grain's surface can make it explode if the electrostatic stress $\epsilon_0 E_0^2$ exceeds the maximum grain's tensile strength against fracture $S$ (e.g. Hill and Mendis, 1979; Draine and Salpeter, 1979). The condition $\epsilon_0 E_0^2 < S$ yields the limiting grain radius

$$a_{\rm nm} > 0.36 \times |Z|^{1/2} (S/10^9 \text{ N m}^{-2})^{-1/4} \tag{40}$$

The maximum tensile strength $S$ of sub-nanometric ice grains is highly uncertain. Since the tensile strength of macroscopic materials is determined in a large part by cracks and dislocations, $S$ is expected to exceed by a large amount the (highly temperature dependent) value of macroscopic ice $S \sim 10^7$ N m$^{-2}$ (Croft et al., 1979), for sub-nanometric grains having a compact structure.

Given these uncertainties and the weak dependence on $S$ of the size limit (40), we make below a tentative order-of-magnitude estimate. With the bonding strength energy $\simeq 0.8 \times 10^{-2}$ eV per hydrogen bond, four hydrogen bonds per water molecule, and assuming bulk water ice density i.e. about $3 \times 10^{28}$ water molecules/m$^3$, we obtain $\sim 2 \times 10^8$ J m$^{-3}$ (equivalent to force per unit area), from which we deduce the tentative strength against fracture $S \sim 2 \times 10^8$ N m$^{-2}$.

Substituting this value in (40) with $Z = 1$ yields the minimum grain radius $a_{\rm min} \simeq 0.7$ nm. This figure varies with the grain's tensile strength $S$ as $S^{-1/4}$, so that varying $S$ by a factor of 5 would produce a variation in $a_{\rm min}$ of about 50%. Note also that 0.7 nm is roughly the size of a unit cell of a Ih ice crystal and twice the width of an elementary step of ice crystallization (Sazaki et al., 2010).

Another size limitation might be produced by the centrifugal stress due to the grain's spin induced by impacts of molecules (Spitzer, 1978; Draine and Salpeter, 1979). Contrary to the above electrostatic limit, it also acts on uncharged grains. At equilibrium (justified by Eq. (42)), the rms angular speed $\omega$ of a grain due to collisions with neutrals of temperature $T_0$ satisfies $I\omega^2 \simeq 3k_B T_0$ where $I \simeq (8/15)\pi\rho a^5$. A spinning grain of mass density $\rho$ will be destroyed if $(\pi/8)\rho a^2 \omega^2 > S$, which yields the survival condition (e.g. Meyer-Vernet, 1984)

$$a_{\rm nm} > 0.5 \times T_{0\rm eV}^{1/3} (S/10^9 \text{ N m}^{-2})^{-1/3} \tag{41}$$

Substituting $T_0 \simeq 0.02$ eV (Waite et al., 2006) and the order of magnitude $S \sim 2 \times 10^8$ N m$^{-2}$ determined above, we obtain $a > 0.2$ nm. Since this limit is smaller than the electrostatic disruption limit (40), centrifugal disruption is not expected to play a major role. Note that we do not consider the spin induced by the impacts of ions of temperature $T$ (although this would yield a size limit higher by the factor $(T/T_0)^{1/3}$), because the ion number density is too small for inducing a significant grain's spin during the time scales involved. Indeed, for the grains to acquire a spin governed by the thermal energy of a particle species, they should have been struck by their own mass of these particles. Applying (5) to $H_2O$ molecules of mass $m_0 \simeq 18 m_p$ yields the time scale

$$\tau_{\rm spin} \simeq \frac{(2\pi)^{1/2}\rho a}{3 n_0 (m_0 k_B T_0)^{1/2}} \sim 10^{10} a_{\rm nm}/(n_{0\rm cm^{-3}} T_{0\rm eV}^{1/2}) \text{ s} \tag{42}$$

whence $\tau_{\rm spin} \sim 1.5 \times 10^3$ s, which is of the order of magnitude of the time scales involved and smaller by more than two orders of magnitude than the value for ion impacts (which confirms that the latter do not affect the grains' spin).

## 6. Concluding remarks

We have derived analytical expressions for the charge of nanograins in cold dense and dusty environments, under conditions relevant in the outer Solar System, and applied them to Enceladus nanograins. This analysis shows that a large proportion of nanograins should be charged with one electron, as assumed in previous studies and argued by Hill et al. (2012), and that the impacts of ambient ions should explain the observed positively charged grains without having to assume other charging processes. Electrostatic stresses are expected to limit the size of charged grains to a minimum radius of about 0.7 nm-a value which should be taken with caution since it assumes a compact structure and varies with the badly known grain tensile strength $S$ in proportion of $S^{-1/4}$. This effect might contribute to the strong decrease in the grain number density observed at radii below about 1 nm (Jones et al., 2009; Hill et al., 2012).

However, subnanometric ice grains fall into the uncertain transition region between macroscopic and microscopic behavior. In particular, the electron sticking coefficient $s_e$ is expected to decrease nearly linearly with radius for $a \lesssim 1$ nm (Vostrikov and Dubov, 2006; Megner and Gumbel, 2009); according to (30) and (34), this should decrease the grain's charge and therefore the probability of detection below $\simeq$1 nm.

Furthermore, the detailed physics of ice crystallization is still not understood, and a grain of radius 1 nm with the density of ice contains only $\simeq 140 H_2O$ molecules, more than 50% of which should lie at the surface. This number is smaller than the recently determined minimum number of 250–300 $H_2O$ molecules required for crystallization of a water cluster (Pradzynski, 2012), which corresponds to a radius of about 1.3 μm with the density of ice. This radius of 1.3 μm (whose dependence on temperature is unknown and which should be taken with caution in the context of Enceladus plume), is close to the observed onset of flux decrease (Jones et al., 2009; Hill et al., 2012).

## Acknowledgments

I thank Tom Hill and another reviewer for their helpful comments on the manuscript.

## References

Abbas, M.M. et al., 2010. Lunar dust charging by electron impact: Complex role of secondary electron emissions in space environments. Astrophys. J. 718, 795–809.
Burns, J.A. et al., 2001. Dusty rings and circumplanetary dust: Observations and simple physics. In: Grün, E. et al. (Eds.), Interplanetary Dust. Springer, pp. 641–715.
Chow, V.W., Mendis, D.A., Rosenberg, M., 1993. Role of grain size and particle velocity distribution in secondary electron emission in space plasmas. J. Geophys. Res. 98, 19065–19076.
Coates, A.J. et al., 2007. Discovery of heavy negative ions in Titan's ionosphere. Geophys. Res. Lett. 34, L22103. http://dx.doi.org/10.1029/2007GL030978.
Cravens, T.E. et al., 2009. Plume ionosphere of Enceladus as seen by the Cassini ion and neutral mass spectrometer. Geophys. Res. Lett. 36, L08106. http://dx.doi.org/10.1029/2009GL037811.
Croft, S.K., Kieffer, S.M., Ahrens, T.J., 1979. Low-velocity impact craters in ice and ice-saturated sand with implications for martian crater count ages. J. Geophys. Res. 84 (B14), 8023–8032.
Dong, Y., Hill, T., 2012. Charged ice grains in the Enceladus plume. In: AGU (Fall Meet.), 3–7 December, San Francisco, Calif.
Dong, Y. et al., 2011. The water vapor plumes of Enceladus. J. Geophys. Res. 116, A10204. http://dx.doi.org/10.1029/2011JA016693.
Draine, B.T., Salpeter, E.E., 1979. On the physics of dust grains in hot gas. Astrophys. J. 231, 77–94.
Draine, B.T., Sutin, B., 1987. Collisional charging of interstellar grains. Astrophys. J. 320, 803–817.
Farrell, W.M. et al., 2010. Modification of the plasma in the near-vicinity of Enceladus by the enveloping dust. Geophys. Res. Lett. 37, L20202. http://dx.doi.org/10.1029/2010GL044768.
Fitting, H.-J. et al., 2001. Attenuation and escape depths of low-energy electron emission. J. Electron Spectrosc. Relat. Phenom. 119, 35–47.
Friedrich, M., Rapp, M., 2009. News from the lower ionosphere: A review of recent developments. Surv. Geophys. 30, 525–559. http://dx.doi.org/10.1007/s10712-009-9074-2.
Garrett, H.B., Hoffman, A.R., 2000. Comparison of spacecraft charging environments at the Earth, Jupiter and Saturn. IEEE Trans. Plasma Sci. 28, 2048–2057.
Gomer, R., 1961. Field Emission and Field Ionisation. Harvard Univ. Press, Cambridge, Mass.
Grard, R.J.L., 1973. Properties of the satellite photoelectron sheath derived from photoemission laboratory measurements. J. Geophys. Res. 78, 2885–2905.
Hansen, C.J. et al., 2008. Water vapour jets inside the plume of gas leaving Enceladus. Nature 456, 477–479.
Havnes, O., Morfill, G.E., Goertz, C.K., 1984. Plasma potential and grain charges in a dust cloud embedded in a plasma. J. Geophys. Res. 89, 10999–11003.
Havnes, O. et al., 1990. On dust charges and plasma potentials in a dusty plasma with dust size distribution. J. Geophys. Res. 95, 6581–6585.
Hill, J.R., Mendis, D.A., 1979. Charged dust in the outer planetary magnetospheres. Moon Planets 21, 3–16.
Hill, T.W. et al., 2012. Charged nanograins in the Enceladus plume. J. Geophys. Res. 117, A05209. http://dx.doi.org/10.1029/2011JA017218.
Horanyi, M., 1996. Charged dust dynamics in the Solar System. Annu. Rev. Astron. Astrophys. 34, 383–418.
Jackson, J.D., 1999. Classical Electrodynamics, third ed. Wiley, p. 61.
Jensen, E.J., Thomas, G.E., 1991. Charging of mesospheric dust particles: Implications for electron density and particle coagulation. J. Geophys. Res. 96 (10), 18603–18615.
Jones, G.H. et al., 2009. Fine jet structure of electrically charged grains in Enceladus plume. Geophys. Res. Lett. 36, L16204. http://dx.doi.org/10.1029/2009GL038284.
Jones, G.H. et al., 2012. Nanodust measured by the Cassini plasma spectrometer. In: Mann, I. et al. (Eds.), Nanodust in the Solar System: Discoveries and Interpretations. Springer, pp. 119–132.
Jurac, S. et al., 1995. Charging of ice grains by low-energy plasmas: Application to Saturn's E ring. J. Geophys. Res. 100 (A8), 14821–14831.
Kempf, S. et al., 2005. Composition of saturnian ring particles. Science 307, 1274–1276. http://dx.doi.org/10.1126/science.1106218.
Kempf, S. et al., 2008. The E ring in the vicinity of Enceladus I. Spatial distribution and properties of the ring particles. Icarus 193, 420–437.
Kimura, Y., 2012. Phenomena of nanoparticles in relation to the Solar System. In: Mann, I., Meyer-Vernet, N., Czechowski, A. (Eds.), Nanodust in the Solar System: Discoveries and Interpretations. Springer, pp. 31–46.
Laframboise, J.G., Parker, L.W., 1973. Probe design for orbit-limited current collection. Phys. Fluids 16, 629–636.
Mann, I., Czechowski, A., 2012. Causes and consequences of the existence of nanodust in interplanetary space. In: Mann, I. et al. (Eds.), Nanodust in the Solar System: Discoveries and Interpretations. Springer, pp. 195–219.
Mann, I. et al., 2011. Dusty plasma effects in near Earth space and interplanetary medium. Space Sci. Rev. 161, 1–47. http://dx.doi.org/10.1007/s11214-011-9762-3.
Mann, I. et al., 2013. Dust in the planetary system. Phys. Rep., in revision.
Megner, L., Gumbel, J., 2009. Charged meteoric particles as ice nuclei in the mesosphere: Part2 – A feasibility study. J. Atmos. Solar-Terr. Phys. 71, 1236–1244.
Mendis, D.A., Axford, W.I., 1974. Satellites and magnetospheres of the outer planets. Annu. Rev. Earth Planet. Sci. 2, 419–474.
Mendis, D.A., Rosenberg, M., 1994. Cosmic dusty plasma. Annu. Rev. Astron. Astrophys. 32, 419–463.
Meyer-Vernet, N., 1982. Flip-flop of electric potential of dust grains in space. Astron. Astrophys. 105, 98–106.
Meyer-Vernet, N., 1984. Some constraints on particles in Saturn's spokes. Icarus 57, 422–431.
Meyer-Vernet, N., 2001. Large scale structure of planetary environments: The importance of not being Maxwellian. Planet. Space Sci. 49, 247–260.
Meyer-Vernet, N. et al., 2009. Dust detection by the wave instrument on STEREO: Nanoparticles picked up by the solar wind? Solar Phys. 256, 463–474.
Michaud, M., Sanche, L., 1987. Total cross-sections for slow-electron (1–20 eV) scattering in solid $H_2O$. Phys. Rev. A 36, 4672–4683.
Morooka, M.W. et al., 2011. Dusty plasma in the vicinity of Enceladus. J. Geophys. Res. 116, A12221. http://dx.doi.org/10.1029/2011JA017038.
Natanson, G.M., 1960. On the theory of the charging of amicroscopic aerosol particles as a result of capture of gas ions. Sov. Phys. Tech. Phys., Engl. Transl. 5, 538–551.
Pierrard, V., Lazar, M., 2010. Kappa distributions: Theory and applications in space plasmas. Solar Phys. 267, 153–174. http://dx.doi.org/10.1007/s11207-010-9640-2.
Pradzynski, C.C., 2012. A fully size-resolved perspective on the crystallization of water clusters. Science 337, 1529–1532.
Rapp, M., Lübken, F.-J., 2001. Modelling of particle charging in the polar summer mesosphere: Part 1 – General results. J. Atmos. Solar-Terr. Phys. 63, 759–770.
Sazaki, G. et al., 2010. Elementary steps at the surface of ice crystals visualized by advanced optical microscopy. Proc. Natl. Acad. Sci. 107, 19702–19707.
Shafiq, M. et al., 2011. Characteristics of the dust–plasma interaction near Enceladus' south pole. Planet. Space Sci. 59, 17–25.
Spahn, F. et al., 2006. Cassini dust measurements at Enceladus and implications for the origin of the E ring. Science 311, 1416–1418.
Spitzer Jr., L., 1978. Physical Processes in the Interstellar Medium. Wiley, p. 185.

Tokar, R.L. et al., 2009. Cassini detection of Enceladus' cold water-group plume ionosphere. Geophys. Res. Lett. 36, L13203. http://dx.doi.org/10.1029/2009GL038923.

Utterback, N.G., Kissel, J., 1990. Attogram dust cloud a million kilometers from Comet Halley. Astron. J. 100, 1315–1322.

Vostrikov, A.A., Dubov, D.Y., 2006. Absolute cross sections of electron attachment to molecular clusters: Part II. Formation of $(H_20)_N^-$, $(N_20)_N^-$, $(N_2)_N^-$. Tech. Phys. 51, 1537–1552.

Waite Jr., J.H. et al., 2006. Cassini ion and neutral mass spectrometer: Enceladus plume composition and structure. Science 311, 1419–1422. http://dx.doi.org/10.1126/science.1121290.

Watson, W.D., 1972. Heating of interstellar HI clouds by ultraviolet photoelectron emission from grains. Astrophys. J. 176, 103–110.

Weingartner, J.C., Draine, B.T., 2001. Photoelectric emission from interstellar dust: Grain charging and gas heating. Astrophys. J. Suppl. Ser. 134, 263–381.

Whipple, E.C., 1981. Potential of surfaces in space. Rep. Prog. Phys. 44, 1197–1250.

Whipple, E.C., Northrop, T.G., Mendis, D.A., 1985. The electrostatics of a dusty plasma. J. Geophys. Res. 90, 7405–7413.

Yaroshenko, V.V. et al., 2009. Characteristics of charged dust inferred from the Cassini RPWS measurements in the vicinity of Enceladus. Planet. Space Sci. 57, 1807–1812.

Zook, H.A., 1996. Solar wind magnetic field bending of jovian dust trajectories. Science 274, 1501–1503.